
Research Article: New Research | Disorders of the Nervous System

Electrophysiological characterization of networks and single cells in the hippocampal region of a transgenic rat model of Alzheimer's disease

Ingrid Heggland^{1,2}, Pål Kvello^{1,3} and Menno P. Witter¹

¹*Kavli Institute for Systems Neuroscience & Centre for Neural Computation, Egil and Pauline Braathen and Fred Kavli Centre for Cortical microcircuits, Norwegian University of Science and Technology (NTNU), Trondheim, NO-7491, Norway*

²*Liaison Committee between the Central Norway Regional Health Authority (RHA), The Norwegian University of Science and Technology (NTNU), Trondheim, NO-7491, Norway*

³*Department of Teacher Education, Norwegian University of Science and Technology (NTNU), Trondheim, NO-7491, Norway*

<https://doi.org/10.1523/ENEURO.0448-17.2019>

Received: 22 December 2017

Revised: 14 November 2018

Accepted: 21 January 2019

Published: 5 February 2019

IH and MPW designed research, IH and PK performed research, IH analyzed data, IH, PK and MPW wrote the paper.

Funding: <http://doi.org/10.13039/100001201Kavli> Foundation

Funding: <http://doi.org/10.13039/501100004590Helse> Midt-Norge (Central Norway Regional Health Authority) 46056620

Funding: Norges Forskningsråd
181676
223262
197467

Funding: Department of Neuroscience, Faculty of Medicine, NTNU

The authors declare no competing financial interests.

Correspondence should be addressed to Menno P. Witter, menno.witter@ntnu.no.

Cite as: eNeuro 2019; 10.1523/ENEURO.0448-17.2019

Alerts: Sign up at www.eneuro.org/alerts to receive customized email alerts when the fully formatted version of this article is published.

Accepted manuscripts are peer-reviewed but have not been through the copyediting, formatting, or proofreading process.

Copyright © 2019 Heggland et al.

This is an open-access article distributed under the terms of the Creative Commons Attribution 4.0 International license, which permits unrestricted use, distribution and reproduction in any medium provided that the original work is properly attributed.

1 **Electrophysiological characterization of networks and single cells in the**
2 **hippocampal region of a transgenic rat model of Alzheimer's disease**

3 Running Title: Electrophysiology of the rat AD hippocampus

4

5 Ingrid Heggland^{1,2}, Pål Kvello^{1,3} and Menno P. Witter^{1*}

6

7 ¹Kavli Institute for Systems Neuroscience & Centre for Neural Computation, Egil and Pauline
8 Braathen and Fred Kavli Centre for Cortical microcircuits, Norwegian University of Science
9 and Technology (NTNU), NO-7491 Trondheim, Norway

10 ²Liaison Committee between the Central Norway Regional Health Authority (RHA) and the
11 Norwegian University of Science and Technology (NTNU), NO-7491 Trondheim, Norway

12 ³Department of Teacher Education, Norwegian University of Science and Technology
13 (NTNU), NO-7491 Trondheim, Norway

14

15 *Corresponding author: Menno P. Witter, Kavli Institute for Systems Neuroscience, Faculty
16 of Medicine and Health Sciences, NTNU, Postboks 8905, NO-7491 Trondheim, Norway.

17 Tel: +47 73598249. Fax: +47 73598294. Email: menno.witter@ntnu.no.

18

19 IH and MPW designed research, IH and PK performed research, IH analyzed data, IH, PK and
20 MPW wrote the paper.

21

22 Number of pages: 50

23 Number of Figures: 5

24 Number of Tables: 6

25 Number of Multimedia: 0

26 Number of words for Abstract: 231

27 Number of words for Significance Statement: 104

28 Number of words for Introduction: 734

29 Number of words for Discussion: 1722

30

31 **Acknowledgements**

32 We thank Dr. A. Claudio Cuello (McGill University, Montreal, Canada) for providing breeding
33 pairs for our colony of McGill-R-Thy1-APP transgenic rats. The authors would also like to
34 thank Hanne T. Soligard for genotyping the rats, and for assistance with histology and
35 immunostaining together with Bruno Monterotti and Stefano Bradamante. Special thanks to
36 Noriko Koganezawa for technical training and advice on the VSDI recordings, Debora
37 Ledergerber for advice and practical help with the electrophysiological recordings, Paulo
38 Girão for assisting with data analysis, Øyvind Salvesen for advice on statistical methods and
39 Maximiliano Jose Nigro for discussions about the manuscript.

40

41 The authors declare no competing financial interests.

42

43 Current affiliation of Ingrid Heggland:

44 Section for Collections and Digital Services, NTNU University Library, Norwegian University of
45 Science and Technology (NTNU), Trondheim, Norway

46

47 **Funding sources**

48 This work was financially supported by the Kavli Foundation, Helse Midt-Norge (grant
49 46056620), The Norwegian Research Council (equipment grant 181676; Centre of Excellence
50 scheme: Centre for Neural Computation, grant 223262 and the National Infrastructure
51 scheme: NORBRAIN1, grant 197467) and the Department of Neuroscience, Faculty of
52 Medicine, Norwegian University of Science and Technology.

53

54 Keywords: voltage-sensitive dye imaging, whole-cell patch clamp, entorhinal cortex,
55 hippocampus, stellate cell, fan cell, intracellular A β , neuronal excitability.

56

57

58 **Abstract**

59 The hippocampus and entorhinal cortex (EC) are areas affected early and severely in
60 Alzheimer's disease (AD), and this is associated with deficits in episodic memory. Amyloid
61 beta ($A\beta$), the main protein found in amyloid plaques, can affect neuronal physiology and
62 excitability, and several AD mouse models with memory impairments display aberrant
63 network activity, including hyperexcitability and seizures. In this study, we investigated
64 single cell physiology in EC and network activity in EC and dentate gyrus in the McGill-R-
65 Thy1-APP transgenic rat model, using whole-cell patch clamp recordings and voltage-
66 sensitive dye imaging in acute slices. In slices from transgenic animals up to 4 months of age,
67 the majority of the principal neurons in layer II of EC, fan cells and stellate cells, expressed
68 intracellular $A\beta$. Whereas the electrophysiological properties of fan cells were unaltered,
69 stellate cells were more excitable in transgenic than in control rats. Stimulation in the
70 dentate gyrus resulted in comparable patterns in both groups at 3 and 9 months, but at 12
71 months, the elicited responses in the transgenic group showed a significant preference for
72 the enclosed blade, without any change in overall excitability. Only transient changes in the
73 local network activity were seen in the medial entorhinal cortex. Although the observed
74 changes in the McGill rat model are subtle, they are specific, pointing to a differential and
75 selective involvement of specific parts of the hippocampal circuitry in $A\beta$ pathology.

76

77

78

79

80

81 **Significance statement**

82 The hippocampal region, essential for episodic memory, is affected in the early stages of
83 Alzheimer's disease. Here, we use the McGill-R-Thy1-APP transgenic rat model to study the
84 effects of A β pathology on networks and single cells in the hippocampal region. In young
85 animals, we observed widespread intracellular A β accumulation, which later progressed to
86 extracellular plaques. However, the in vitro physiology was largely unaltered, with only
87 changes in single cell excitability of stellate cells in layer II of MEC and network activation
88 patterns in dentate gyrus. Thus, these two components of the entorhinal-hippocampal
89 network emerge as potentially more vulnerable in the context of A β pathology.

90

91 **Introduction**

92 Alzheimer's disease (AD), the most common cause of dementia, is a progressive
93 neurodegenerative disorder. The neuropathological hallmarks include extracellular amyloid
94 plaques and intracellular neurofibrillary tangles consisting of hyperphosphorylated tau, as
95 well as cortical atrophy and cell loss. Areas affected by plaques and tangles in early stages of
96 AD include the entorhinal cortex (EC) and the hippocampus (Braak & Braak, 1991; Thal et al.,
97 2002). Neuron loss has been reported in subregions of the hippocampus (West et al., 1994;
98 Simic et al., 1997; Price et al., 2001), and in particular layer II of EC exhibits a substantial cell
99 loss in patients in the early stages of AD as well as with mild cognitive impairment (Gomez-
100 Isla et al., 1996; Kordower et al., 2001). The two main groups of principal neurons in layer II,
101 stellate cells in medial EC (MEC) and fan cells in lateral EC (LEC) (Canto & Witter, 2012a; b),
102 provide input to the hippocampus via the perforant path (Cappaert et al., 2015). In
103 transgenic mice, it has been shown that both tau and amyloid- β (A β) pathology can spread

104 through transsynaptic transmission, starting in EC (Harris et al., 2010; de Calignon et al.,
105 2012), further implicating the entorhinal-hippocampal region in early stages of AD.

106

107 The original “amyloid cascade hypothesis” was formulated 25 years ago (Hardy & Higgins,
108 1992). Although the exact role of A β in the initiation and progression of AD is still highly
109 debated, it is clear that A β is an important contributor to the pathological processes (Herrup,
110 2015; Musiek & Holtzman, 2015). The research focus has shifted to include effects of soluble
111 forms of A β (Haass & Selkoe, 2007) and A β peptide levels have been shown to have a higher
112 correlation with cognitive decline than amyloid plaque load does (McLean et al., 1999;
113 Naslund et al., 2000). Studies have shown toxic effects of A β oligomers on synaptic function
114 and structure (Selkoe, 2008; Marchetti & Marie, 2011), which could lead to disruption of the
115 normal neuronal function and subsequent aberrant network activity (Palop & Mucke,
116 2010a). Recent studies report changes in single neuron excitability in mouse models,
117 including pyramidal cells of CA1 (Brown et al., 2011; Kerrigan et al., 2014), and frontal cortex
118 (Kellner et al., 2014), as well as EC (Marcantoni et al., 2013; Xu et al., 2015) and dentate
119 gyrus (DG) (Hazra et al., 2013). Additionally, intracellular delivery of A β has been shown to
120 increase neuronal excitability (Scala et al., 2015), and intracellular A β (iA β) is found in EC and
121 hippocampus of AD patients (Gouras et al., 2000; D'Andrea et al., 2002). As intracellular
122 accumulation and cognitive deficits have been observed in animal models prior to formation
123 of plaques (Billings et al., 2005; Leon et al., 2010), it is hypothesized that iA β may play an
124 important role in neuronal dysfunction in AD (Bayer & Wirths, 2010).

125

126 In this study we use the McGill-R-Thy1-APP transgenic rat model which harbors human
127 amyloid β precursor protein (A β PP) with the Indiana and Swedish double mutations (Leon et

128 al., 2010), and is one of the few rat models with a progressive plaque pathology. The first
129 plaques appear in the subiculum at 9 months of age and then spread to other parts of the
130 hippocampus as well as EC (Hegglund et al., 2015). A subtle cell loss (~20%) has also been
131 reported in the subiculum at 18 months (Hegglund et al., 2015). By one week after birth, iA β
132 is observed (Leon et al., 2010), and layer II of EC is one of the areas with initial high
133 expression (Kobro-Flatmoen et al., 2016). From 3 months, the rats display cognitive
134 impairments (Iulita et al., 2014) and metabolic alterations (Nilsen et al., 2014), and pre-
135 plaque inflammation and changes in long-term potentiation have been described at later
136 ages (Hanzel et al., 2014; Qi et al., 2014). In the present study, we investigated changes in
137 excitability and activity patterns of the networks of the hippocampus and EC in acute slices.
138 We used young pre-plaque animals, when only iA β accumulation is present, as well as older
139 animals, when plaques have started to appear. With the use of whole-cell patch clamp
140 recording in acute slices from young animals, we investigated possible changes in the
141 excitability of stellate and fan cells in layer II of EC. We also assessed whether changes in
142 electrophysiological properties at the network level were related to the developing
143 pathology over time, with the use of voltage sensitive dye imaging (VSDI).
144

145 **Materials and methods**

146 ***Animals***

147 All the experimental procedures were approved by the Local Animal Research Authority and
148 followed the European Convention for the Protection of Vertebrate Animals used for
149 Experimental and Other Scientific Purposes. The animals were kept on a 12 hour light/dark
150 cycle under standard laboratory conditions (19-22°C, 50-60% humidity) and had free access
151 to food and water. A colony of transgenic McGill-R-Thy1-APP rats, based on two breeding
152 pairs obtained from McGill University (Leon et al., 2010), was maintained at our university.
153 The McGill-R-Thy1-APP rats carries the human $A\beta PP_{751}$ including the Swedish double
154 mutation and the Indiana mutation under the control of the *Thy1.2* promoter. Quantitative
155 PCR (qPCR) was used to decide the genotype of the transgenic rats (negative, homozygous or
156 hemizygous for the transgene). Genomic DNA was isolated from samples of ear tissue with a
157 High Pure PCR Template Preparation Kit (11796828001, Roche Diagnostics, Basel,
158 Switzerland). The transgene (human A β PP) and a normalization gene (GAPDH or beta-actin)
159 were detected using RT² qPCR Primer Assays from Qiagen (PPH05947A, PPR06557 and
160 PPR06570C, Venlo, Netherlands) with FastStart Universal SYBR Green Master (04913850001,
161 Roche Diagnostics) on an Applied Biosystems StepOnePlus real-time PCR system (Life
162 Technologies Ltd, Thermo Fisher Scientific, Waltham, MA, USA). The $\Delta\Delta C_T$ values were
163 calculated from the qPCR with a known homozygous sample as reference (Livak &
164 Schmittgen, 2001).

165

166 ***Slice preparation***

167 For the VSDI, homozygous (+/+) transgenic rats and wild type control animals (wt;
168 WistarHan, Taconic, Hudson, NY, USA) of both sexes at the ages of 3, 9 and 12 months were

169 used. For whole-cell patch clamp recordings, homozygous (+/+) transgenic rats and negative
170 (-/-) littermates of both sexes at the ages of 1 and 3-4 months were included. The animals
171 were anesthetized with isoflurane (IsoFlo vet., Abbott Laboratories, Chicago, IL, USA),
172 decapitated and the brain quickly removed from the skull and placed in ice-cold (0-4°C),
173 oxygenated (95% O₂/5% CO₂) artificial cerebrospinal fluid (ACSF) solution containing (in
174 mM): 100 D-Mannitol, 119 choline chloride, 2.5 KCl, 7 MgCl₂, 0.5 CaCl₂, 25 Glucose, 1.25
175 NaH₂PO₄, 25 NaHCO₃, 11.5 sodium ascorbate and 3 sodium pyruvate. For rats of 3 months
176 and older, a transcardial perfusion with ice-cold ACSF was done before decapitation, to
177 remove blood and cool down the brain as quickly as possible.

178

179 For VSDI, the brain was cut in 400 µm thick horizontal entorhinal-hippocampal slices on a
180 vibratome (Vibratome 300 sectioning system, Vibratome, IL, USA). Slices ranged from
181 approximate interaural levels 2.4 to 4.68 mm (Paxinos & Watson, 2007), containing mid to
182 ventral levels of the hippocampus. The slices were placed on a membrane filter
183 (JHWP01300, Omnipore membrane filter, PTFE, Merck Millipore, Darmstadt, Germany) glued
184 to a thin Plexiglas ring (11 mm inner diameter, 15 mm outer diameter) and held in a
185 oxygenated moist interface chamber at 32°C for at least one hour before transfer to the
186 recording chamber. For holding and recording, the following ACSF was used (in mM): 126
187 NaCl, 3 KCl, 2 MgSO₄, 2 CaCl₂, 10 glucose, 1.2 NaH₂PO₄, 26 NaHCO₃.

188

189 For whole-cell patch clamp recordings, entorhinal slices of 400 µm were cut on a vibratome
190 (Leica VT1000S, Leica Biosystems, Nussloch, Germany), either in the horizontal or
191 semicoronal plane (20° angle with the vertical plane). Horizontal slices from middle
192 dorsoventral levels, approximately interaural 2.9 to 4.4 mm (Paxinos & Watson, 2007) were

193 used for recording MEC II cells, with the majority of the recorded cells found in the center of
194 the mediolateral axis within each slice. Semicoronal slices were used for recording LEC II cells
195 close to the rhinal fissure, at approximate rostrocaudal levels of 4.3 to 6 mm posterior to
196 bregma (Paxinos & Watson, 2007). The slices were held in a submersion chamber with ACSF
197 containing (in mM): 126 NaCl, 3 KCl, 3 MgCl₂, 0.5 CaCl₂, 10 glucose, 1.2 NaH₂PO₄, 26 NaHCO₃
198 at 37°C for one hour, and then at room temperature until recording.

199

200 ***Voltage-sensitive dye imaging***

201 The slice was perfused with oxygenated ACSF at 34°C in a recording chamber mounted on a
202 fluorescent microscope (Axio Examiner.D1, Carl Zeiss, Oberkochen, Germany), and stained
203 with the voltage-sensitive dye RH 795 (0.5mg/ml ACSF; R-649, Molecular Probes, Invitrogen,
204 Life Technologies, Thermo Fisher Scientific, Waltham, MA, USA) for 3 minutes and the excess
205 dye was washed out by perfusion of ASCF for 15 minutes before recording. The slice was
206 illuminated from a halogen lamp (MHAB-150W, Moritex, Saimata, Japan) through a
207 bandpass excitation filter (535 ± 25 nm) and a dichroic mirror (half reflectance wavelength of
208 580 nm) and the dye emission was passed through a longpass filter (50% transmittance at
209 590) and detected with a CMOS-camera (100 x 100 pixel array; MiCAM Ultima, Brainvision,
210 Tokyo, Japan). For the 3 month age group a non-immersion Zeiss Fluor objective was used
211 (NA = 0.25). For the 9 and 12 month groups a water-immersion objective from Brainvision
212 (NA = 0.35) was used, as we obtained this after the 3 month group was recorded. A shutter
213 (HL-151, Brainvision) controlled by the Brainvision acquisition software built into the light
214 source was opened 500ms before the start of the recording to reduce mechanical noise. The
215 images were acquired at 1.0 ms/frame for 512 frames and the first 50 frames were used to
216 measure the optical baseline. An extracellular stimulation was applied after 50 ms with a

217 tungsten bipolar electrode (tip separation of 150 μm) using either a single pulse with an
218 amplitude of 0.2 or 0.6 mA of 300 μs duration, or 4 pulses at a frequency of 40 Hz with an
219 amplitude of 0.2 mA. Eight recordings separated by 3 seconds were averaged to reduce
220 noise. The stimulation electrode was placed in different areas of the hippocampal region:
221 the border of the molecular and granule layer of the DG and layers II/III of entorhinal. In the
222 9 and 12 month age group the majority of the slices (38 of 44 slices) were also recorded with
223 the GABA_A antagonist bicuculline added to the ACSF (5 μM ; Bicuculline methiodide; 14343,
224 Sigma-Aldrich, St Louis, MO, USA), to block the inhibition in the slice.

225

226 ***Whole-cell patch clamp***

227 All single cell recordings were performed at 34°C with perfusion of oxygenated ACSF
228 containing (in mM): 126 NaCl, 3 KCl, 1.5 MgCl₂, 1.6 CaCl₂, 10 glucose, 1.2 NaH₂PO₄, 26
229 NaHCO₃. Principal cells in layer II of MEC and LEC were identified using infrared differential
230 interference contrast (IR-DIC) on an Axio Examiner.D1 microscope (Carl Zeiss, Oberkochen,
231 Germany) with a Zeiss Plan-Apochromat water dipping objective (20x; NA = 1.0), or an
232 Olympus BX51WI microscope (Olympus, Tokyo, Japan) with an Olympus LC Plan FL objective
233 (40x; NA = 0.8). Recording pipettes pulled from standard-walled borosilicate capillaries (3-8
234 M Ω pipette resistance; GC120F-10, Harvard Apparatus, Harvard Bioscience, Holliston, MA,
235 USA) were filled with intracellular solution containing (in mM): 120 K-gluconate, 10 KCl, 10
236 HEPES, 4 MgATP, 10 Na₂-phosphocreatine, 0.3 GTP. Biocytin (3-4%; B4261, Sigma-Aldrich, St
237 Louis, MO, USA) was added to the recording solution for later anatomical analysis of cell
238 location and morphology. For a few of the cells (n = 34 cells) an Alexa Fluor hydrazide dye
239 (405, 488, 468 or 633; Molecular Probes, Invitrogen, Life Technologies, Thermo Fisher
240 Scientific, Waltham, MA, USA) was added to the intracellular solution instead of biocytin.

241 Whole-cell recordings in current clamp mode were performed on two different setups.
242 Recordings on the first setup was done with MultiClamp 700A and 700B amplifiers (Axon
243 Instruments, Molecular Devices, Sunnyvale, CA, USA) in bridge mode and digitized with an
244 InstruTECH ITC-1600 A/D interface (HEKA Elektronik, Lambrecht, Germany) in combination
245 with the acquisition software Chartmaster (HEKA). The second setup was equipped with a
246 Multiclamp 700B amplifier and data was acquired with an InstruTECH ITC-18 board (HEKA)
247 and the acquisition software Patchmaster (HEKA; RRID: SCR_000034). Recordings were made
248 at sampling rates of 10, 25 or 50 kHz, depending on the length of the recording. Capacitance
249 compensation was maximal and series resistance was compensated, and the seal resistance
250 was above 1 G Ω . We did not correct for the liquid junction potential, which was calculated to
251 be 15.8 mV.

252

253 To study general electrophysiological properties and firing frequencies of neurons, voltage
254 responses to a series of 1 s long current steps of 50 or 30 pA starting from – 300pA were
255 recorded. A protocol of 10 pA steps starting from 0 pA was used to measure the rheobase. In
256 addition, we injected a sinusoidal current with a linearly increasing frequency (from 0 to 20
257 Hz) with a duration of 15 seconds, a so-called ZAP-protocol (Erchova et al., 2004), while
258 recording the membrane voltage, and estimated the resonance frequency (frequency with
259 largest amplitude response). In 11 cells, the resonance frequency could not be estimated,
260 due to traces with noise or action potentials.

261

262

263

264

265 ***Histology***

266 After recordings, the slices were fixed for minimum 24 hours in 4% freshly depolymerized
267 paraformaldehyde (w/v in 125 mM phosphate buffer (PB), pH 7.4) and then transferred to
268 20 % glycerol and 2% dimethyl sulfoxide (DMSO) in 125 mM PB.

269

270 The slices from VSDI were subsequently cut at 50 μm on a freezing microtome (Microm
271 HM430, Thermo Fischer Scientific, Waltham, MA, USA). Half of the sections were mounted
272 directly on Histobond⁺ slides and stained with Cresyl violet to verify the regions of activity
273 seen with the VSDI. After drying overnight on a heating plate (37 °C) the sections were
274 dehydrated in ethanol, cleared in xylene and rehydrated before staining with Cresyl violet (1
275 g/L) for 10-15 minutes. The sections were then alternately dipped in ethanol-acetic acid (5
276 mL acetic acid in 1 L 70% ethanol) and rinsed with cold water until the desired differentiation
277 was obtained, then dehydrated, cleared in xylene and coverslipped with Entellan (Merck
278 KGaA, Darmstad, Germany).

279

280 The other half of the sections were stained with free-floating immunohistochemistry using
281 the monoclonal anti-human A β antibody McSA1 (MM-0015-P; MédiMabs, Montreal, QC,
282 Canada; RRID: AB_1807985;), which is specific for human A β and stains both plaques and
283 intracellular deposits (Grant et al., 2000; Leon et al., 2010). First, heat-induced epitope
284 retrieval was done at 60 °C for 2 h in PB. After washing with PB (2x10 minutes) the tissue was
285 permeabilized with 0.5% Triton-X-100 in Tris-buffered saline (TBS-Tx; 50 mM Tris, 150 mM
286 NaCl, pH 8.0) for 10 minutes and blocked with 10% goat serum in TBS-Tx for 30 minutes,
287 before overnight incubation at 4 °C with the primary antibody, McSA1 (1:4000). The
288 following day, the sections were washed with TBS-Tx (3x10 minutes) and incubated with a

289 biotinylated goat anti-mouse secondary antibody (1:200, Sigma-Aldrich) for 90 minutes.
290 After washing (TBS-Tx; 3x10 minutes), incubation in ABC (PK-4000, Vectastain ABC kit,
291 Vector Laboratories, Burlingame, CA, USA) for 90 minutes, washing with TBS-Tx (3x10
292 minutes) and Tris-HCl (50 mM Tris adjusted to pH 7.6 with HCl; 2x5 minutes) and the
293 sections were incubated in 0.67% diaminobenzidine (DAB) with 0.024% H₂O₂ in Tris-HCl for
294 30 minutes. After a final wash with Tris-HCl (2x5 minutes) the sections were mounted on
295 Superfrost slides, dried overnight on heating plates, cleared with xylene and coverslipped
296 with Entellan. A Zeiss Axio Imager.M1 microscope (Carl Zeiss) with a CX9000 camera (MBF
297 Bioscience, Williston, VT, USA) was used to take brightfield photomicrographs of the
298 sections, which were further processed with Adobe Photoshop CS6 (Adobe Systems, San
299 Jose, CA, USA; RRID:SCR_014199).

300

301 The slices from single-cell recordings were processed to visualize the morphology of the cells
302 and to determine the intracellular expression of A β . Heat-induced epitope retrieval (HIER)
303 was applied at 60 °C for 2 h in PB and the slices were then washed 2x15 min in PB at room
304 temperature followed by 5x15 min wash in 0.5% Triton-X-100 in TBS-Tx and incubation with
305 the primary antibody, McSA1 (1:1000), at 4 °C for 4 days. After rinsing 5x15 in TBS-Tx the
306 slices were incubated overnight in room temperature with Alexa Fluor 488 conjugated to
307 streptavidin (1:300; S11223) and a goat anti-mouse secondary antibody conjugated with
308 Alexa Fluor 546 (1:200; A11003, Molecular Probes). A subset of the slices was stained with
309 the opposite combination of fluorophores (Alexa Fluor 546 streptavidin, S11225 and Alexa
310 Fluor 488 goat anti-mouse, A11001). Subsequently, the sections were washed 3 x 15 min
311 with TBS-Tx, mounted and coverslipped. The slices were scanned using a laser scanning
312 confocal microscope (LSCM; LSM 510, Carl Zeiss) to determine the cell morphology and

313 intracellular expression of A β . Alexa 488 was excited by an Argon/2 laser and the emission
314 was registered through a 505-550 bandpass filter, whereas Alexa 546 was excited by a DPSS
315 461-10 laser and the emission was bandpass filtered at 575-615.

316

317 ***Analysis of VSDI data***

318 The Brainvision analysis software (BV_Ana) was used to analyze the optical signals. Changes
319 in membrane potential cause proportional changes in the emission of the voltage sensitive
320 dye (Grinvald et al., 1988), and these were evaluated as fractional changes in the fluorescent
321 signal ($\Delta F/F$). All the optical signals were processed using spatial and cubic filters in BV_Ana.
322 The first 50 frames were used as the average baseline, and the fractional optical signals were
323 color-coded and superimposed on a brightfield image to represent the spread of neural
324 activity in the slice (Fig. 1A). In the recordings from DG stimulation we quantified the neural
325 activation by calculating the integral (area under the curve) from optical traces in voxels in
326 the molecular layer of DG and CA3, as this measure would represent the magnitude of the
327 total membrane potential changes (Koganezawa et al., 2008). In addition, the total activated
328 area in the whole slice after DG stimulation was quantified as the total number of pixels
329 above threshold, with the threshold set to be 0.05% $\Delta F/F$. The paired-pulse ratio (PPR) was
330 calculated by dividing the maximal amplitude of second pulse by the first pulse, with a pulse
331 interval of 25 ms. This was done for the voxels in each of the two blades of DG and an overall
332 average PPR for DG was calculated for each slice. In recordings with stimulation in superficial
333 MEC, stripes of voxels were analyzed. This was done both across layers and within the
334 superficial layers in MEC, to evaluate the spread of the signal in the local network (Fig. 1B).

335

336

337 ***Analysis of whole-cell patch clamp data***

338 Analysis of the whole-cell current-clamp recordings was performed using the software
339 Fitmaster (HEKA). The input resistance was calculated from the steady-state voltage
340 response to injected current steps that did not elicit action potentials (APs) by fitting the
341 quadratic equation:

$$342 \quad \Delta V = R_{N,0}\Delta I + c_{AR}\Delta I^2$$

343 Where $R_{N,0}$ is the voltage-independent input resistance and c_{AR} is the coefficient of
344 anomalous rectification (Waters & Helmchen, 2006). The membrane time constant, τ , was
345 estimated by fitting a double exponential to the voltage response of a -300 pA current
346 injection and using the higher value. The rebound potential was measured from a -300 pA
347 current step (if the trace did not include a rebound AP), as the difference between the
348 maximal value after the end of the stimulus (V_{max}) and the baseline measured before the
349 start of the stimulus ($V_{baseline}$). The sag ratio was defined as:

$$350 \quad Sag = (V_{baseline} - V_{ss}) / (V_{baseline} - V_{min})$$

351 where V_{min} is the minimal value reached after the onset of the stimulus and V_{ss} is the steady-
352 state value of the voltage response to a -300 pA current step. The resting membrane
353 potential (V_m) was estimated by averaging a 10 s spontaneous recording. The following
354 action potential parameters were estimated from the first action potential of the rheobase
355 trace (the first trace in the rheobase protocol to elicit an AP): AP threshold (defined as
356 maximum of the double derivative of the voltage response, found using a fit), AP amplitude
357 (difference between maximum amplitude and AP threshold), AP half width (width at 50% of
358 max AP amplitude), fast afterhyperpolarization potential (fAHP; minimum value directly after
359 AP) and the depolarizing afterpotential (DAP; difference between the maximum value after
360 the AP and the fAHP, in five cells with doublet spikes this could not be measured). The

361 parameters fAHP and DAP were only measured in cells from MEC LII. We calculated AP
362 amplitude, AP width at 0 mV and interspike interval (ISI) as a function of AP number from a
363 positive current step (+200 or 210 pA), as well as the ratio between the first and the second
364 ISI and the adaptation ratio ($ISI_{\text{first}}/ISI_{\text{last}}$). To look at the relationship between firing
365 frequency and current we measured the average firing frequency from current steps ranging
366 from 200 to 500 pA. We also measured the instantaneous frequency between the two first
367 APs (f_0) and the two last APs (steady state, f_{ss}). The afterhyperpolarization potential (AHP)
368 after the end of the current injection was also measured, for current steps ranging from 50
369 to 500 pA. The measures of firing frequencies and AHP as a function of current were only
370 done on a subset of the cells, and for MEC this dataset only included cells from the 1 month
371 old animals. Cells that had a $V_m > -57$ mV, AP amplitude < 75 mV or a bridge balance > 22 M Ω
372 were excluded from the analysis, as well as putative interneurons.

373

374 The images from the LSCM were used to classify the neurons based on morphology. Cells in
375 LEC LII that had a clear pyramidal ($n = 9$) or multiform ($n = 17$) morphology and cells in MEC
376 LII with a clear pyramidal ($n = 7$) morphology, but not the intermediate cells types, were
377 excluded from the analysis. Some cells were not filled well enough with biocytin to visualize
378 the morphology ($n = 9$ for LEC and $n = 5$ for MEC). As the vast majority of the cells that were
379 filled sufficiently were classified as fan cells (101 of 127 cells in LECII; 80%) or stellate cells
380 (73 of 80 cells in MECII; 91%), we assumed that most of the non-filled cells would be of these
381 types, and these were therefore included in the analysis. All the included cells from MEC
382 displayed the known typical electrophysiological properties of stellate cells, including
383 prominent sag and rebound.

384

385 ***Statistical analysis***

386 The quantitative VSDI data obtained in DG and MEC, was analyzed with respect to effect of
387 genotype within each age group using a linear mixed model. Fixed factors were sex,
388 genotype (+/+ or wild type) and where relevant, area (exposed and enclosed blade of DG) or
389 distance from electrode in MEC, as well as the interaction between genotype and
390 area/distance from electrode. A repeated effects variable with a diagonal or compound
391 symmetry covariance structure (chosen based on convergence and information criteria) was
392 included to account for several voxels (the regions of interest) being measured in each slice
393 (intraslice variance).

394

395 A linear mixed model was used to estimate the effect of genotype on the measured
396 electrophysiological parameters from the single cell recordings. Rat ID was added as a
397 random effect to account for several cell recordings within one animal, and thus the values
398 from each cell will not be independent. Genotype and age were included as fixed effects
399 with two levels each (+/+ and -/-; 1 month and 3 months). In addition sex and experimental
400 setup was included as a fixed effect to correct for possible differences that might bias the
401 results. An extended model was also run to test for the possible interactions between
402 genotype and age, and genotype and sex. On parameters with several measurements within
403 the same cell (e.g. for several APs or current steps) the AP number or injected current was
404 included as factors and as repeated measures with cell ID as the subject variable. The
405 covariance structure for the repeated measures was compound symmetry or unstructured,
406 based on which one had lower information criteria. The possible interaction between
407 genotype and AP number or genotype and injected current was also included in the
408 statistical model.

409

410 No corrections were done for multiple testing and results were considered statistically
411 significant when $p < 0.05$. IBM SPSS Statistics, version 22 (IBM Corporation, New York, USA;
412 RRID: SCR_002865) was used for the statistical analysis.

413

414 **Results**

415 *No changes in fan cell physiology in lateral entorhinal cortex and subtle changes in stellate* 416 *cell physiology in the medial entorhinal cortex in homozygous McGill-R-Thy1-APP rats*

417

418 To investigate whether basic electrophysiological properties or firing behavior were altered
419 in the McGill-R-Thy1-APP transgenic rat, we performed whole-cell patch-clamp recordings in
420 the current clamp mode of principal cells in layer II of LEC and MEC in rats aged 1 and 3-4
421 months of age.

422

423 We included 111 fan cells from LEC in the electrophysiological analysis ($n = 47$ cells from
424 transgenic animals and $n = 64$ cells from control animals; aged 1 and 3-4 months). Since $iA\beta$
425 reportedly aggregates preferentially in LEC close to the rhinal fissure (Kobro-Flatmoen et al.,
426 2016), we selectively recorded fan cells in LEC superficially in layer II and just ventral to the
427 rhinal fissure, in semicoronal slices (Fig. 2A). Most of them displayed the typical morphology,
428 with apical dendrites fanning out towards the pial surface and only a few or no basal
429 dendrites (Tahvildari & Alonso, 2005; Canto & Witter, 2012a; Fig. 2B). Fan cells showed a low
430 sag and rebound potential, no spike doublets/triplets or DAP, but had a relatively high input
431 resistance and time constant (Fig. 2C; Canto & Witter, 2012a; b). The majority of the fan cells

432 recorded in homozygous (+/+) transgenic rats (89%; 31 of 35 neurons) stained positive for
433 intracellular A β (Fig. 2G). A few neurons in the +/+ animals were not A β immunoreactive (4
434 of 35 fan cells; example in fig. 2H), whereas in negative littermates (-/-) none of the neurons
435 showed immunoreactivity to human A β .

436

437 None of the measured basic electrophysiological or action potential parameters of fan cells
438 differed between the transgenic and control animals (Table 1 and Extended Data Table 1.1).
439 Similarly, there was no significant effect of genotype on the measured waveform parameters
440 and firing properties (Table 2 and Extended Data Table 2.1).

441

442 In total, 78 stellate cells in layer II of MEC were included in the analysis (n = 38 cells from
443 homozygous transgenic rats and n = 40 cells from negative littermates, aged 1 and 3-4
444 months). The stellate cells, recorded in horizontal slices, were mainly located superficially in
445 layer II (Fig. 2D), and not at extremes of the mediolateral axis (i.e. not close to the border to
446 parasubiculum or LEC). The majority of the stellate cells displayed the typical morphology,
447 with dendrites radiating from the soma (Fig. 2E), though some cells had intermediate stellate
448 to pyramidal morphologies (Canto & Witter, 2012b; Fuchs et al., 2016). All included cells
449 showed a prominent sag (low sag ratio) and rebound potential, and rebound spikes after a
450 hyperpolarizing pulse were not uncommon (Fig. 2F). In addition spike doublets or triplets
451 could be seen in the start of spiking trains, and a fAHP and DAP was clearly seen after single
452 APs (Canto & Witter, 2012b). When staining for intracellular A β , 96% of the recorded stellate
453 cells in slices from transgenic were A β -immunoreactive (25 of 26 cells; example in fig. 2I). No
454 A β -immunoreactive neurons were observed in the control slices (Fig. 2J).

455

456 Of all the electrophysiological properties measured in stellate cells, two parameters were
457 altered in transgenic compared to control rats (Tables 3 and 4, Extended Tables. 3.1 and 4.1).
458 The fAHP displayed a slight but significantly increased hyperpolarization in the homozygous
459 +/- rats compared to the controls (Table 3, row k), and f_0 was also significantly increased in
460 the +/- transgenic rats (Table 4, row g; estimated effect 36.2 Hz).

461 In the statistical model, age and sex were included as fixed effects, and on several of the
462 electrophysiological parameters these had significant effects (Tables 1-3). In this study, the
463 aim was to investigate the effects of genotype, but these results for age and sex underline
464 the importance of including these as factors in the statistical analyses.

465

466 ***Voltage-sensitive dye imaging and A β immunoreactivity of the hippocampal region***

467 In view of the minor increase in excitability observed in layer II stellate cells in MEC,
468 combined with the fact that these neurons provide major inputs to the DG (Cappaert et al.,
469 2015), we decided to record the propagation of neural activity in the hippocampal region
470 using VSDI in acute brain slices of McGill-R-Thy1-APP and wild type rats (Fig. 1). Bipolar
471 electrical stimulation was applied to the dentate gyrus and medial entorhinal cortex (areas
472 shown with red asterisks in Fig. 3A). The slices used for VSDI were also immuno-stained for
473 A β -42 and showed that in wild type animals staining was absent (Fig. 3B, D and E), whereas
474 every transgenic animal in all age groups (3, 9, and 12 months) had strong intracellular A β
475 immunoreactivity in several areas of the hippocampal region (Fig. 3C, F and G). Expression
476 was particularly strong in the pyramidal cell layer of subiculum (Fig. 3F), CA1, CA3 (Fig. 3C) as
477 well as in layer II of the entorhinal cortex (Fig. 3G). No extracellular plaques were seen in any

478 of the slices from animals aged 3 or 9 months, whereas at 12 months the plaque levels were
479 highly variable, from no plaques to very high plaque loads (Heggland et al., 2015).

480

481

482 ***The neural network responses in the two blades of DG show subtle alterations in***

483 ***transgenic rats***

484 Stimulation in the molecular layer in the crest of DG, the area bridging the two blades, with a
485 single pulse (0.2 mA for 300 μ s), resulted in activation in both of the blades of DG as well as
486 in the hilus, and in several cases a small change in the optical signal could also be seen in CA3
487 (Fig. 4). In the wild type animals, the exposed blade (also called the outer, free or
488 infrapyramidal blade) had a higher level of activity than the enclosed blade (also called the
489 inner or suprapyramidal blade), at all ages (Fig. 4, left panels). In the homozygous transgenic
490 animals, this pattern of activation was also seen in the majority of the slices at 3 and 9
491 months (Fig. 4, right panels). However, at 12 months of age, we observed that some
492 transgenic rats had larger responses in the enclosed than the exposed blade or very similar
493 responses in the two blades after stimulation in the crest (Fig. 4, lower right panel).

494

495 Quantification of the membrane potential changes were in line with this altered pattern of
496 DG activation, following single pulse stimulation (Fig. 5; Extended Data Fig 5.1). At 3 and 9
497 months, there was a larger membrane potential change in the exposed blade than the
498 enclosed blade in both wild type and control animals (Fig. 5A, left and middle panel). The
499 statistical analysis, using the mixed linear model, showed a significant effect of area (blade)
500 at 3 and 9 months, but no significant effect of genotype or interaction between area and
501 genotype (Extended Data Figure 5.1, row a and b). At 12 months, the effect of area was no

502 longer significant, nor was there a main effect of genotype (Extended Data Figure 5.1, row c).
503 However, at 12 months there was a significant interaction between genotype and area
504 (Extended Data Figure 5.1, row c) and the membrane potential changes in the enclosed
505 blade were significantly higher in the homozygous transgenic animals than in the wild type
506 animals (Fig. 5A, right panel). The same pattern of activation in DG was also found when
507 stimulating with 4 pulses at 40 Hz, and with the addition of the GABA_A antagonist bicuculline
508 (Fig. 5B, middle and right panels). The statistical test showed comparable results, with a
509 significant interaction between genotype and area at 12, but not 9 months (Extended Data
510 Figure 5.1, rows d-g).

511

512 In all age groups the total activated area (number of pixels) was unaltered in the +/+
513 transgenic rats compared to wild type (Table 5). In addition, there was no significant
514 difference between the PPR in wild type and +/+ transgenic animals at either 9 or 12 months
515 (Table 5). The addition of bicuculline did not change this pattern of activation. This indicates
516 that although there was a change in the activation pattern of DG in the homozygous
517 transgenic animals at 12 months, the overall excitability of the DG circuitry was not altered.

518

519

520 ***Transient changes in neural network responses in MEC in transgenic rats***

521

522 Layer II neurons in MEC that project to the hippocampus, also give rise to local axon
523 collaterals in layer I and II, reaching for around 300 μm with an occasional spread of up to
524 400 μm along the transverse axis (Tamamaki and Nojyo, 1993; Klink and Alonso, 1997;
525 Schmidt et al., 2017). These local collaterals may innervate neurons in layers II, III and V,

526 since all have apical dendrites in layers I/II. We therefore aimed to look at differences in local
527 network responses between wild type and transgenic animals upon stimulation in layer II in
528 MEC using VSDI.

529

530 Stimulation in superficial MEC (single 0.6 mA pulse) led to changes in the VSDI signal that
531 spread in the superficial layers as well as to the deep layers of MEC (Example image in Fig.
532 1A). In addition, small changes were observed in the pre- and parasubiculum and DG in
533 many slices. We analyzed changes in fluorescent signal in individual voxels taken at the
534 position of the stimulation electrode and gradually moving away with a maximum distance
535 of approximately 700 μm away from the electrode. As expected, a significant effect of
536 distance from electrode was seen, with a decreasing signal with distance both across and
537 within layers (Table 6; Extended Table 6.1). No main effect of genotype was observed for any
538 age group (Table 6). However, at 3 months there was a significant interaction between
539 genotype and distance from electrode across layers, but this was not seen at 9 and 12
540 months (Table 6). Similarly, a small but significant interaction between genotype and
541 distance from electrode within layers was seen at 9 months, but not 3 and 12 months (Table
542 6). These significant interactions indicate alterations in the network responses in the MEC of
543 the transgenic rats. However, the effects are small and transient, as they are only seen in
544 single age groups.

545

546

547 **Discussion**

548 Accumulating evidence suggests that the cognitive symptoms of memory loss and learning
549 impairments in the early stages of AD are not mainly due to neuronal loss or atrophy, but
550 can be linked to neuronal and synaptic dysfunction and subsequent abnormal patterns of
551 activation in local neuronal circuits and larger-scale networks (D'Amelio & Rossini, 2012). A β
552 peptides likely play an important role in these deleterious processes by affecting synapses
553 and synaptic function (Palop & Mucke, 2010b). Here, we studied changes in the entorhinal-
554 hippocampal network and single cells in acute slices taken from McGill-R-Thy1-APP
555 transgenic rats expressing human mutated APP. We first analyzed the electrophysiological
556 properties and excitability of the main principal cell populations in layer II of EC, fan cells and
557 stellate cells, with the use of *in vitro* whole-cell patch clamp. When comparing transgenic
558 rats and controls, at 1 month and 3-4 months of age, we found no alterations in any of the
559 passive membrane properties, and only subtle differences in the excitability of stellate cells.
560 Further, with the use of VSDI, we observed alterations in the activation patterns of the two
561 blades of DG in 12 months old homozygous transgenic animals, as well as transient changes
562 in the local network activity in MEC.

563

564 Other studies report network hyperexcitability, including seizures, in different brain areas of
565 several mouse models of AD (Palop et al., 2007; Minkeviciene et al., 2009; Harris et al., 2010;
566 Verret et al., 2012), including EC (Duffy et al., 2015; Xu et al., 2015) and DG (Hazra et al.,
567 2013). In the current study, we did not find clear evidence for generalized hyperexcitability
568 of EC or DG in the McGill rat using VSDI in slices. This apparent discrepancy likely is caused
569 by the different experimental methods used. The optical signals we recorded represent the
570 averaged membrane voltage changes in the total population of cells, including glial cells. An

571 increased number of hyperactive as well as hypoactive neurons has previously been
572 reported in AD mice using Ca^{2+} -imaging (Busche et al., 2008; Busche et al., 2012). Such
573 changes in single cells or ensembles would sum together and would therefore be difficult, if
574 not impossible, to detect with VSDI. In addition, many of the studies reporting aberrant
575 network activity in transgenic AD models have been done in vivo, with techniques including
576 EEG (Minkeviciene et al., 2009; Verret et al., 2012), single neuron (Kellner et al., 2014) or
577 local field potential recordings (Xu et al., 2015). Thus, we cannot exclude the possibility that
578 in vivo recordings or utilizing a different method to assess network function might reveal
579 other changes in the McGill-R-Thy1-APP rat not seen in the present study.

580

581 We found no alterations of subthreshold intrinsic properties in either fan cell or stellate cells
582 in the homozygous transgenic McGill rats aged 1 and 3-4 months. In Tg2576 mice, fan and
583 stellate cells in EC showed no changes in the input resistance and resting membrane
584 potential (Marcantoni et al., 2013), in agreement with our findings. Similar results with no
585 changes in subthreshold properties have been shown in pyramidal cells in CA1 of the McGill
586 rat (Qi et al., 2014), PSAPP (Brown et al., 2011), PDAPP (Kerrigan et al., 2014), 3xTg-AD (Scala
587 et al., 2015) and CRND8 mice (Wykes et al., 2012) as well as in the frontal cortex of
588 APP^{swe}/PS1^{dE9} (APdE9) mice (Kellner et al., 2014). In contrast, a depolarization of the
589 resting membrane potential has been found in interneurons in DG and pyramidal cells in
590 neocortex in APdE9 mice (Minkeviciene et al., 2009; Hazra et al., 2013) in addition to
591 parvalbumin-positive interneurons, but not pyramidal cells in parietal cortex of hAPPJ20
592 mice (Verret et al., 2012), suggesting that cell populations might be differentially affected.

593

594 We identified two suprathreshold properties that showed alterations in stellate cells in the
595 homozygous rats. Stellate cells display a clear fAHP followed by a DAP (Alonso & Klink, 1993)
596 and this fAHP is due to a Ca^{2+} -dependent K^+ conductance (Storm, 1987; Klink & Alonso,
597 1993). This conductance is thought to be mediated by BK (big potassium) channels, and is
598 also important for spike repolarization (Sah, 1996). The BK channels can facilitate high-
599 frequency firing, likely through limiting the activation of other potassium channels and
600 decreasing the inactivation of sodium channels (Gu et al., 2007). Notably, the BK current is
601 transient, inactivating rapidly, and thus will be most influential in the initial part of a spike
602 train (Shao et al., 1999). Correspondingly, the other alteration we observed in stellate cells in
603 the transgenic rats was increased excitability early in the spike train, a slightly higher f_0 at 1
604 month. It is thus possible that the hyperexcitability we here describe in the MEC stellate cells
605 in the McGill rat actually results from early changes in ion conductances, in particular the BK
606 potassium current, which might worsen over time. Whether the BK channel, or other
607 channels, are affected specifically in this model, will be of interest for further studies. Several
608 studies report various physiological alterations of single cells in other transgenic mouse
609 models, including changes in excitability, potassium currents and AP waveform (Brown et al.,
610 2011; Wykes et al., 2012; Kerrigan et al., 2014; Scala et al., 2015), highlighting several
611 possible channels as targets for $\text{A}\beta$ toxicity.

612

613 The VSDI data indicates an alteration of the response pattern in DG, seen in the 12 month
614 homozygous transgenic group, but not at 3 and 9 months. The McGill-R-Thy1-APP rat initially
615 displays extracellular plaques at around 9 months, and although the pattern of plaque
616 deposition is similar across animals, the age of onset and temporal progression of the plaque
617 pathology varied considerably between animals (Hegglund et al., 2015). This corresponds to

618 the findings in the current study, with highly variable levels of plaque in the recorded slices
619 from the different homozygous transgenic animals. It is of interest to mention that one
620 animal with the highest plaque load also had the largest change in DG activation pattern. In
621 AD mice models, hyperactive neurons have been found to be associated with plaques
622 (Busche et al., 2008; Busche et al., 2012) and deficits in place cell firing were related to
623 hippocampal plaque burden in the Tg2576 model (Cacucci et al., 2008). Consistent with this
624 are findings that synaptic density is reduced in proximity to plaques (Dong et al., 2007) and
625 neurons in contact with plaques have a loss of perisomatic GABAergic synapses (Garcia-
626 Marin et al., 2009), providing a possible mechanism for some of the observed network
627 changes in AD models.

628

629 The observed responses after stimulation in the molecular layer of DG, which is a major area
630 of termination of the perforant path input from layer II of EC, revealed an asymmetry in the
631 activation of the two blades in wild type animals, with larger amplitudes in the exposed
632 (infrapyramidal) blade than in the enclosed (suprapyramidal) blade. A similar asymmetry has
633 been reported previously with VSDI in rats (Scharfman et al., 2002; Wright & Jackson, 2014)
634 and Ca^{2+} imaging in mice (Yu et al., 2013). The inhibitory circuitry differs in the two blades
635 (Seress & Pokorny, 1981), which could be a possible explanation for these observations.

636 However, the asymmetry, as well as the alterations seen in the 12 month transgenic group,
637 were seen using both normal ACSF and after addition of the GABA_A receptor antagonist
638 bicuculline. This indicates that differences or alterations in inhibition do not play a major role
639 in this case, although effects of GABA_B cannot be completely ruled out. Other known blade
640 differences include the perforant path input from the entorhinal cortex, with the two blades
641 receiving preferential input from different parts of EC (Wyss, 1981; Witter et al., 1989).

642 Although the precise distribution of the perforant path to the two blades is somewhat
643 disputed (Witter et al., 1989), these anatomical differences might play a role in the
644 asymmetric activation of DG.

645

646 Although possible sex differences were not the focus of this study, the observed effects do
647 support the inclusion of sex as a factor in future studies. In the statistical analysis of the
648 electrophysiological parameters, we included age and sex as factors, both to be able to
649 account for possible bias on the estimated effect of genotype, as well as the possibility that
650 genotype had a differential effect on either sex or with increasing age. Women are at higher
651 risk of developing Alzheimer's disease (Li & Singh, 2014) and sex differences have been
652 described in other animal models of AD (Wang et al., 2003). An effect of sex on changes in
653 metabolism has been described in the McGill-R-Thy1-APP rat (Nilsen et al., 2014) although
654 no clear differences were reported between males and females regarding plaque pathology
655 (Heggland et al., 2015) or memory impairments (Leon et al., 2010). Some of the possible
656 effects we find here might be due to different, and fluctuating, hormone levels, but also
657 differences in genes and gene expression between sexes could play a part (Shah et al., 2014)
658 The effects seen with age were also in general minor. Since we recorded in rats aged 1
659 month (juvenile) and 3-4 months (adult), the changes could reflect the transition to
660 adulthood. Previously, stellate cells in MEC of young adult (postnatal day 46) rats have been
661 shown to be less excitable, and have slight alterations in intrinsic electrophysiological
662 properties, compared to juvenile (postnatal day 21) rats (Boehlen et al., 2010).

663

664

665 In summary, we found that in young animals, there were only minor alterations in the
666 intrinsic electrophysiological parameters of single cells, with a slight hyperexcitability seen in
667 stellate cells and no changes in the fan cells in the homozygous rats, although the majority of
668 these cells displayed accumulation of $iA\beta$. Following up on this, we found that the networks
669 of DG and MEC were largely unaltered in the McGill-R-Thy1-APP transgenic rat. However, at
670 12 months there was a statistically significant change in the typically asymmetric activation
671 of the DG seen in wild type rats. Additionally, there were transient changes in the local
672 network of MEC. Whether the hyperexcitability of stellate cells plays a major role in the
673 cognitive deficits seen in pre-plaque homozygous McGill rats still remains an open question.
674 Additionally, the results from the VSDI point to the possible involvement of the medial
675 perforant path to the DG in AD dysfunction. Even small alterations in the EC-DG or intrinsic
676 DG circuitry could therefore perturb the normal hippocampal processing and thus affect
677 learning and memory.
678

679 **References**

680

681

682 Alonso A & Klink R (1993) Differential electroresponsiveness of stellate and pyramidal-like cells of
683 medial entorhinal cortex layer II. *J Neurophysiol* 70:128-143.

684 Bayer TA & Wirths O (2010) Intracellular accumulation of amyloid-Beta - a predictor for synaptic
685 dysfunction and neuron loss in Alzheimer's disease. *Front Aging Neurosci* 2:8.

686 Billings LM, Oddo S, Green KN, McGaugh JL & LaFerla FM (2005) Intraneuronal Abeta causes the
687 onset of early Alzheimer's disease-related cognitive deficits in transgenic mice. *Neuron*
688 45:675-688.

689 Boehlen A, Heinemann U & Erchova I (2010) The range of intrinsic frequencies represented by medial
690 entorhinal cortex stellate cells extends with age. *J Neurosci* 30:4585-4589.

691 Braak H & Braak E (1991) Neuropathological staging of Alzheimer-related changes. *Acta*
692 *Neuropathol* 82:239-259.

693 Brown JT, Chin J, Leiser SC, Pangalos MN & Randall AD (2011) Altered intrinsic neuronal excitability
694 and reduced Na⁺ currents in a mouse model of Alzheimer's disease. *Neurobiol Aging* 32:2109
695 e2101-2114.

696 Busche MA, Chen X, Henning HA, Reichwald J, Staufenbiel M, Sakmann B & Konnerth A (2012) Critical
697 role of soluble amyloid-beta for early hippocampal hyperactivity in a mouse model of
698 Alzheimer's disease. *Proc Natl Acad Sci U S A* 109:8740-8745.

699 Busche MA, Eichhoff G, Adelsberger H, Abramowski D, Wiederhold KH, Haass C, Staufenbiel M,
700 Konnerth A & Garaschuk O (2008) Clusters of hyperactive neurons near amyloid plaques in a
701 mouse model of Alzheimer's disease. *Science* 321:1686-1689.

702 Cacucci F, Yi M, Wills TJ, Chapman P & O'Keefe J (2008) Place cell firing correlates with memory
703 deficits and amyloid plaque burden in Tg2576 Alzheimer mouse model. *Proc Natl Acad Sci U*
704 *S A* 105:7863-7868.

- 705 Canto CB & Witter MP (2012a) Cellular properties of principal neurons in the rat entorhinal cortex. I.
706 The lateral entorhinal cortex. *Hippocampus* 22:1256-1276.
- 707 Canto CB & Witter MP (2012b) Cellular properties of principal neurons in the rat entorhinal cortex. II.
708 The medial entorhinal cortex. *Hippocampus* 22:1277-1299.
- 709 Cappaert NL, Van Strien NM & Witter MP (2015) Hippocampal Formation. In: *The Rat Nervous*
710 *System, Fourth Edition* (Paxinos G, ed), pp511-573. Academic Press.
- 711 D'Amelio M & Rossini PM (2012) Brain excitability and connectivity of neuronal assemblies in
712 Alzheimer's disease: from animal models to human findings. *Prog Neurobiol* 99:42-60.
- 713 D'Andrea MR, Nagele RG, Wang HY & Lee DH (2002) Consistent immunohistochemical detection of
714 intracellular beta-amyloid42 in pyramidal neurons of Alzheimer's disease entorhinal cortex.
715 *Neurosci Lett* 333:163-166.
- 716 de Calignon A, Polydoro M, Suarez-Calvet M, William C, Adamowicz DH, Kopeikina KJ, Pitstick R,
717 Sahara N, Ashe KH, Carlson GA, Spires-Jones TL & Hyman BT (2012) Propagation of tau
718 pathology in a model of early Alzheimer's disease. *Neuron* 73:685-697.
- 719 Dong H, Martin MV, Chambers S & Csernansky JG (2007) Spatial relationship between synapse loss
720 and beta-amyloid deposition in Tg2576 mice. *J Comp Neurol* 500:311-321.
- 721 Duffy AM, Morales-Corraliza J, Bermudez-Hernandez KM, Schaner MJ, Magagna-Poveda A, Mathews
722 PM & Scharfman HE (2015) Entorhinal cortical defects in Tg2576 mice are present as early as
723 2-4 months of age. *Neurobiol Aging* 36:134-148.
- 724 Erchova I, Kreck G, Heinemann U & Herz AV (2004) Dynamics of rat entorhinal cortex layer II and III
725 cells: characteristics of membrane potential resonance at rest predict oscillation properties
726 near threshold. *J Physiol* 560:89-110.
- 727 Fuchs EC, Neitz A, Pinna R, Melzer S, Caputi A & Monyer H (2016) Local and Distant Input Controlling
728 Excitation in Layer II of the Medial Entorhinal Cortex. *Neuron* 89:194-208.

- 729 Garcia-Marin V, Blazquez-Llorca L, Rodriguez JR, Boluda S, Muntane G, Ferrer I & Defelipe J (2009)
730 Diminished perisomatic GABAergic terminals on cortical neurons adjacent to amyloid
731 plaques. *Front Neuroanat* 3:28.
- 732 Gomez-Isla T, Price JL, McKeel DW, Jr., Morris JC, Growdon JH & Hyman BT (1996) Profound loss of
733 layer II entorhinal cortex neurons occurs in very mild Alzheimer's disease. *J Neurosci*
734 16:4491-4500.
- 735 Gouras GK, Tsai J, Naslund J, Vincent B, Edgar M, Checler F, Greenfield JP, Haroutunian V, Buxbaum
736 JD, Xu H, Greengard P & Relkin NR (2000) Intraneuronal Abeta42 accumulation in human
737 brain. *Am J Pathol* 156:15-20.
- 738 Grant SM, Ducatenzeiler A, Szyf M & Cuello AC (2000) Abeta immunoreactive material is present in
739 several intracellular compartments in transfected, neuronally differentiated, P19 cells
740 expressing the human amyloid beta-protein precursor. *J Alzheimers Dis* 2:207-222.
- 741 Grinvald A, Frostig RD, Lieke E & Hildesheim R (1988) Optical imaging of neuronal activity. *Physiol Rev*
742 68:1285-1366.
- 743 Gu N, Vervaeke K & Storm JF (2007) BK potassium channels facilitate high-frequency firing and cause
744 early spike frequency adaptation in rat CA1 hippocampal pyramidal cells. *J Physiol* 580:859-
745 882.
- 746 Haass C & Selkoe DJ (2007) Soluble protein oligomers in neurodegeneration: lessons from the
747 Alzheimer's amyloid beta-peptide. *Nat Rev Mol Cell Biol* 8:101-112.
- 748 Hanzel CE, Pichet-Binette A, Pimentel LS, Iulita MF, Allard S, Ducatenzeiler A, Do Carmo S & Cuello AC
749 (2014) Neuronal driven pre-plaque inflammation in a transgenic rat model of Alzheimer's
750 disease. *Neurobiol Aging* 35:2249-2262.
- 751 Hardy JA & Higgins GA (1992) Alzheimer's disease: the amyloid cascade hypothesis. *Science* 256:184-
752 185.

- 753 Harris JA, Devidze N, Verret L, Ho K, Halabisky B, Thwin MT, Kim D, Hamto P, Lo I, Yu GQ, Palop JJ,
754 Masliah E & Mucke L (2010) Transsynaptic progression of amyloid-beta-induced neuronal
755 dysfunction within the entorhinal-hippocampal network. *Neuron* 68:428-441.
- 756 Hazra A, Gu F, Aulakh A, Berridge C, Eriksen JL & Ziburkus J (2013) Inhibitory neuron and hippocampal
757 circuit dysfunction in an aged mouse model of Alzheimer's disease. *PLoS One* 8:e64318.
- 758 Heggland I, Storkaas IS, Soligard HT, Kobro-Flatmoen A & Witter MP (2015) Stereological estimation
759 of neuron number and plaque load in the hippocampal region of a transgenic rat model of
760 Alzheimer's disease. *Eur J Neurosci* 41:1245-1262.
- 761 Herrup K (2015) The case for rejecting the amyloid cascade hypothesis. *Nat Neurosci* 18:794-799.
- 762 Iulita MF, Allard S, Richter L, Munter LM, Ducatenzeiler A, Weise C, Do Carmo S, Klein WL, Multhaup
763 G & Cuello AC (2014) Intracellular Abeta pathology and early cognitive impairments in a
764 transgenic rat overexpressing human amyloid precursor protein: a multidimensional study.
765 *Acta Neuropathol Commun* 2:61.
- 766 Kellner V, Menkes-Caspi N, Beker S & Stern EA (2014) Amyloid-beta alters ongoing neuronal activity
767 and excitability in the frontal cortex. *Neurobiol Aging* 35:1982-1991.
- 768 Kerrigan TL, Brown JT & Randall AD (2014) Characterization of altered intrinsic excitability in
769 hippocampal CA1 pyramidal cells of the Abeta-overproducing PDAPP mouse.
770 *Neuropharmacology* 79:515-524.
- 771 Klink R & Alonso A (1993) Ionic mechanisms for the subthreshold oscillations and differential
772 electroresponsiveness of medial entorhinal cortex layer II neurons. *J Neurophysiol* 70:144-
773 157.
- 774 Klink R & Alonso A (1997) Morphological characteristics of layer II projection neurons in the rat
775 medial entorhinal cortex. *Hippocampus* 7:571-83.
- 776 Kobro-Flatmoen A, Nagelhus A & Witter MP (2016) Reelin-immunoreactive neurons in entorhinal
777 cortex layer II selectively express intracellular amyloid in early Alzheimer's disease. *Neurobiol*
778 *Dis* 93:172-183.

- 779 Koganezawa N, Taguchi A, Tominaga T, Ohara S, Tsutsui K, Witter MP & Iijima T (2008) Significance of
780 the deep layers of entorhinal cortex for transfer of both perirhinal and amygdala inputs to
781 the hippocampus. *Neurosci Res* 61:172-181.
- 782 Kordower JH, Chu Y, Stebbins GT, DeKosky ST, Cochran EJ, Bennett D & Mufson EJ (2001) Loss and
783 atrophy of layer II entorhinal cortex neurons in elderly people with mild cognitive
784 impairment. *Ann Neurol* 49:202-213.
- 785 Leon WC, Canneva F, Partridge V, Allard S, Ferretti MT, DeWilde A, Vercauteren F, Atifeh R,
786 Ducatenzeiler A, Klein W, Szyf M, Alhonen L & Cuello AC (2010) A novel transgenic rat model
787 with a full Alzheimer's-like amyloid pathology displays pre-plaque intracellular amyloid-beta-
788 associated cognitive impairment. *J Alzheimers Dis* 20:113-126.
- 789 Li R & Singh M (2014) Sex differences in cognitive impairment and Alzheimer's disease. *Front*
790 *Neuroendocrinol* 35:385-403.
- 791 Livak KJ & Schmittgen TD (2001) Analysis of relative gene expression data using real-time quantitative
792 PCR and the 2^{-Delta Delta C(T)} Method. *Methods* 25:402-408.
- 793 Marcantoni A, Raymond EF, Carbone E & Marie H (2013) Firing properties of entorhinal cortex
794 neurons and early alterations in an Alzheimer's disease transgenic model. *Pflugers Arch*.
- 795 Marchetti C & Marie H (2011) Hippocampal synaptic plasticity in Alzheimer's disease: what have we
796 learned so far from transgenic models? *Rev Neurosci* 22:373-402.
- 797 McLean CA, Cherny RA, Fraser FW, Fuller SJ, Smith MJ, Beyreuther K, Bush AI & Masters CL (1999)
798 Soluble pool of Abeta amyloid as a determinant of severity of neurodegeneration in
799 Alzheimer's disease. *Ann Neurol* 46:860-866.
- 800 Minkeviciene R, Rheims S, Dobszay MB, Zilberter M, Hartikainen J, Fulop L, Penke B, Zilberter Y,
801 Harkany T, Pitkanen A & Tanila H (2009) Amyloid beta-induced neuronal hyperexcitability
802 triggers progressive epilepsy. *J Neurosci* 29:3453-3462.
- 803 Musiek ES & Holtzman DM (2015) Three dimensions of the amyloid hypothesis: time, space and
804 'wingmen'. *Nat Neurosci* 18:800-806.

- 805 Naslund J, Haroutunian V, Mohs R, Davis KL, Davies P, Greengard P & Buxbaum JD (2000) Correlation
806 between elevated levels of amyloid beta-peptide in the brain and cognitive decline. *JAMA*
807 283:1571-1577.
- 808 Nilsen LH, Melo TM, Witter MP & Sonnewald U (2014) Early differences in dorsal hippocampal
809 metabolite levels in males but not females in a transgenic rat model of Alzheimer's disease.
810 *Neurochem Res* 39:305-312.
- 811 Palop JJ, Chin J, Roberson ED, Wang J, Thwin MT, Bien-Ly N, Yoo J, Ho KO, Yu GQ, Kreitzer A,
812 Finkbeiner S, Noebels JL & Mucke L (2007) Aberrant excitatory neuronal activity and
813 compensatory remodeling of inhibitory hippocampal circuits in mouse models of Alzheimer's
814 disease. *Neuron* 55:697-711.
- 815 Palop JJ & Mucke L (2010a) Amyloid-beta-induced neuronal dysfunction in Alzheimer's disease: from
816 synapses toward neural networks. *Nat Neurosci* 13:812-818.
- 817 Palop JJ & Mucke L (2010b) Synaptic depression and aberrant excitatory network activity in
818 Alzheimer's disease: two faces of the same coin? *Neuromolecular Med* 12:48-55.
- 819 Paxinos G & Watson C (2007) *The Rat Brain in Stereotaxic Coordinates*, 6th edition. Academic Press,
820 Elsevier Inc.
- 821 Price JL, Ko AI, Wade MJ, Tsou SK, McKeel DW & Morris JC (2001) Neuron number in the entorhinal
822 cortex and CA1 in preclinical Alzheimer disease. *Arch Neurol* 58:1395-1402.
- 823 Qi Y, Klyubin I, Harney SC, Hu N, Cullen WK, Grant MK, Steffen J, Wilson EN, Do Carmo S, Remy S,
824 Fuhrmann M, Ashe KH, Cuello AC & Rowan MJ (2014) Longitudinal testing of hippocampal
825 plasticity reveals the onset and maintenance of endogenous human A β -induced synaptic
826 dysfunction in individual freely behaving pre-plaque transgenic rats: rapid reversal by anti-
827 A β agents. *Acta Neuropathol Commun* 2:175.
- 828 Scala F, Fusco S, Ripoli C, Piacentini R, Li Puma DD, Spinelli M, Laezza F, Grassi C & D'Ascenzo M
829 (2015) Intraneuronal A β accumulation induces hippocampal neuron hyperexcitability

- 830 through A-type K(+) current inhibition mediated by activation of caspases and GSK-3.
831 Neurobiol Aging 36:886-900.
- 832 Scharfman HE, Sollas AL, Smith KL, Jackson MB & Goodman JH (2002) Structural and functional
833 asymmetry in the normal and epileptic rat dentate gyrus. J Comp Neurol 454:424-439.
- 834 Schmidt H, Gour A, Straehle J, Boergens KM, Brecht M & Helmstaedter M (2017) Axonal synapse
835 sorting in medial entorhinal cortex. Nature 549:469-475.
- 836 Selkoe DJ (2008) Soluble oligomers of the amyloid beta-protein impair synaptic plasticity and
837 behavior. Behav Brain Res 192:106-113.
- 838 Seress L & Pokorny J (1981) Structure of the granular layer of the rat dentate gyrus. A light
839 microscopic and Golgi study. J Anat 133:181-195.
- 840 Shah K, McCormack CE & Bradbury NA (2014) Do you know the sex of your cells? Am J Physiol Cell
841 Physiol 306:C3-18.
- 842 Shao LR, Halvorsrud R, Borg-Graham L & Storm JF (1999) The role of BK-type Ca²⁺-dependent K⁺
843 channels in spike broadening during repetitive firing in rat hippocampal pyramidal cells. J
844 Physiol 521 Pt 1:135-146.
- 845 Simic G, Kostovic I, Winblad B & Bogdanovic N (1997) Volume and number of neurons of the human
846 hippocampal formation in normal aging and Alzheimer's disease. J Comp Neurol 379:482-
847 494.
- 848 Storm JF (1987) Action potential repolarization and a fast after-hyperpolarization in rat hippocampal
849 pyramidal cells. J Physiol 385:733-759.
- 850 Tamamaki N, Nojyo Y (1993) Projection of the entorhinal layer II neurons in the rat as revealed by
851 intracellular pressure-injection of neurobiotin. Hippocampus 3:471-80.
- 852 Tahvildari B & Alonso A (2005) Morphological and electrophysiological properties of lateral
853 entorhinal cortex layers II and III principal neurons. J Comp Neurol 491:123-140.
- 854 Thal DR, Rub U, Orantes M & Braak H (2002) Phases of A beta-deposition in the human brain and its
855 relevance for the development of AD. Neurology 58:1791-1800.

856 Verret L, Mann EO, Hang GB, Barth AM, Cobos I, Ho K, Devidze N, Masliah E, Kreitzer AC, Mody I,
857 Mucke L & Palop JJ (2012) Inhibitory interneuron deficit links altered network activity and
858 cognitive dysfunction in Alzheimer model. *Cell* 149:708-721.

859 Wang J, Tanila H, Puolivali J, Kadish I & van Groen T (2003) Gender differences in the amount and
860 deposition of amyloidbeta in APPswe and PS1 double transgenic mice. *Neurobiol Dis* 14:318-
861 327.

862 Waters J & Helmchen F (2006) Background synaptic activity is sparse in neocortex. *J Neurosci*
863 26:8267-8277.

864 West MJ, Coleman PD, Flood DG & Troncoso JC (1994) Differences in the pattern of hippocampal
865 neuronal loss in normal ageing and Alzheimer's disease. *Lancet* 344:769-772.

866 Witter MP, Groenewegen HJ, Lopes da Silva FH & Lohman AH (1989) Functional organization of the
867 extrinsic and intrinsic circuitry of the parahippocampal region. *Prog Neurobiol* 33:161-253.

868 Wright BJ & Jackson MB (2014) Long-term potentiation in hilar circuitry modulates gating by the
869 dentate gyrus. *J Neurosci* 34:9743-9753.

870 Wykes R, Kalmbach A, Eliava M & Waters J (2012) Changes in the physiology of CA1 hippocampal
871 pyramidal neurons in preplaque CRND8 mice. *Neurobiol Aging* 33:1609-1623.

872 Wyss JM (1981) An autoradiographic study of the efferent connections of the entorhinal cortex in the
873 rat. *J Comp Neurol* 199:495-512.

874 Xu W, Fitzgerald S, Nixon RA, Levy E & Wilson DA (2015) Early hyperactivity in lateral entorhinal
875 cortex is associated with elevated levels of AbetaPP metabolites in the Tg2576 mouse model
876 of Alzheimer's disease. *Exp Neurol* 264:82-91.

877 Yu EP, Dengler CG, Frausto SF, Putt ME, Yue C, Takano H & Coulter DA (2013) Protracted postnatal
878 development of sparse, specific dentate granule cell activation in the mouse hippocampus. *J*
879 *Neurosci* 33:2947-2960.

880

881 **Figure legends**

882 **Figure 1.** A) Example of VSDI imaging with stimulation in MECII in a horizontal slice (top) and
883 the corresponding Nissl stain after histology (bottom). B) Illustration of regions of interest
884 (stripes) chosen to analyzed the VSDI signals in MEC, across layer (top left) and within the
885 superficial layers (bottom left). To the right the corresponding traces for the voxels along the
886 stripe is shown with the traces taken from the three color-coded voxels represented with
887 the corresponding color.

888

889 **Figure 2.** The characteristic morphology and electrophysiology of a fan cell and a stellate cell
890 from entorhinal cortex layer II and examples of intracellular expression of human A β in
891 recorded cell. A) Representative example of a semicoronal slice used for recording cells in
892 LEC. The asterisk ventral to the rhinal fissure marks the location of the patched cell shown in
893 (B). B) Confocal image showing the morphology of a typical fan cell in layer II of LEC, close to
894 the rhinal fissure (location marked in A). C) Trace from the fan cell in (B) showing voltage
895 responses to hyperpolarizing and depolarizing current steps of ± 300 pA. D) Representative
896 example of a horizontal slice used for recording cells in the MEC. The asterisk marks the
897 location of the cell shown in (E). E). Confocal image showing the morphology of a typical
898 stellate cell in layer II if MEC (location marked in D). F) Trace from the stellate cell in (E)
899 showing voltage responses to hyperpolarizing and depolarizing current steps of ± 300 pA.
900 LEC, lateral entorhinal cortex; MEC, medial entorhinal cortex. G) Confocal scan from a 3
901 months old homozygous McGill-R-Thy1-APP transgenic rat showing a fan cell in LEC LII with
902 intracellular A β . H) Confocal scan from a 1 month old homozygous transgenic rat showing a
903 stellate cell in MEC LII with intracellular A β . I) Confocal scan from a 1 month old homozygous
904 transgenic rat showing a fan cell in LEC LII without expression of intracellular A β . J) Confocal

905 scan from a 1 month old negative control animal showing no expression of human
906 intracellular A β . The cells were filled with biocytin during recording and visualized with
907 streptavidin labeled with Alexa Fluor 488. The presence of the anti-human A β antibody
908 McSA1 was visualized with Alexa Fluor 546. LEC, lateral entorhinal cortex; MEC, medial
909 entorhinal cortex.

910

911 **Figure 3.** Horizontal slices from control animals and homozygous McGill-R-Thy1-APP rats
912 were used for VSDI. A) Example of a horizontal slice stained with cresyl violet showing the
913 different areas targeted for stimulation (red asterisks). B) Example slice from a 9 months old
914 wild type rat showing no immunoreactivity against A β , using the human-specific anti-A β
915 antibody McSA1. C) Example slice from a 12 months old homozygous transgenic rat with
916 intracellular A β immunoreactivity. Insets show higher magnification of the subiculum (D, F)
917 and the medial entorhinal cortex (E, G). Scale bars: 500 μ m (bar in A represents all overview
918 images, bar in D all insets).

919

920

921 **Figure 4.** Voltage sensitive dye imaging of DG showed differences in activation patterns in
922 control and transgenic animals. Evoked activity from a bipolar stimulation electrode (single
923 0.2 mA pulse) centered in DG in control (left) and transgenic (right) animals. The activity
924 spread to both blades, and in some cases activity could also be seen in CA3. At 3 and 9
925 months, the membrane potential changes were in general larger in the exposed blade than
926 the enclosed blade. In contrast, at 12 months several of the transgenic animals showed an
927 increased activity in the inner blade. Images are from representative horizontal slices from
928 wild type and +/- transgenic animals at 3, 9 and 12 months of age. Scale bars: 500 μ m

929

930 **Figure 5.** The evoked activity in the two blades of DG was significantly altered in 12 months
931 old transgenic animal, with increased activity in the enclosed blade, with a constant overall
932 activated area. A) Quantification of the relative membrane potential change measured with
933 VSDI in the two blades of DG (ROI are the voxels shown in figure 3) is shown for 3, 9 and 12
934 months. In control animals the majority of the slices had larger membrane potential changes
935 in the exposed blade than the enclosed blade, but at 12 months this pattern was altered in a
936 portion of the transgenic animals, while the total activated area was similar in all age groups.
937 Asterisk indicates estimated marginal means that have non-overlapping 95% confidence
938 intervals. B) Quantification of the relative membrane potential change measured with VSDI
939 in the two blades of DG and CA3 in transgenic and control animals after a single or 4 pulse
940 stimulation and in the presence of 5 μ M bicuculline at 9 and 12 months. At 9 months the
941 pattern of activation was similar in transgenic and control animals (top panels), but at 12
942 months this pattern was altered in the +/+ transgenic group (bottom panels). For each age
943 group the effects of genotype and area and the interaction was tested with a linear mixed
944 model. Results from the statistical analysis are shown in Extended Data Figure 5.1

945

946

947

948 **Tables**

949

950

951

952 **Table 1.** Results from the mixed linear model analysis for electrophysiological parameters of LEC II
 953 fan cells in homozygous transgenic animals (+/+) and controls (-/-). Basic electrophysiological and
 954 action potential properties from all individual cells are represented in Extended Data Table 1.1.

		Estimated marginal		p-values for test of fixed effects		
		means				
		-/-	+/+	Genotype	Age	Sex
a	Input resistance (M Ω)	138.0	129.8	0.299	0.085	0.013 ¹
b	Time constant, τ (ms)	28.9	30.7	0.230	0.746	0.001 ²
c	Sag ratio	0.803	0.799	0.776	0.284	0.890
d	Rebound (mV)	5.45	5.51	0.926	0.534	0.666
e	V_m (mV)	-69.3	-70.7	0.126	0.022 ³	0.204
f	Rheobase (pA)	71	72	0.934	0.034 ⁴	0.006 ⁵
g	AP threshold (mV)	-45.0	-46.8	0.054	0.313	0.119
h	AP amplitude (mV)	91.8	91.7	0.898	0.563	0.098
i	AP half width (ms)	1.071	1.128	0.152	0.665	0.659

955 n = 111 cells from 40 animals. V_m , resting membrane potential; AP, action potential.

956 ¹Effect size: 21.9 M Ω (males higher) ²Effect size: 5.6 ms (males higher) ³Effect size: -2.2 mV ⁴Effect size: 18.9 pA

957 ⁵Effect size: 24.5 pA (males lower)

958

959

960

961 **Table 2.** Estimated p-values for action potential parameters as a function of AP number and firing
 962 properties of LEC LII fan cells. Action potential and firing properties of LEC LII fan cells in homozygous
 963 transgenic rats (+/+) and control animals (-/-) are shown in Extended Data Table 2.1.

964

		Genotype	Age	Sex	AP no	AP*Genotype
a	AP amplitude	0.855	0.002 ¹	0.024 ²	0.000	0.059
b	AP width	0.388	0.195	0.620	0.000	0.123
c	ISI	0.166	0.124	0.039 ³	0.000	0.317
d	ISI1/ISI2	0.698	0.007 ⁴	0.006 ⁵	-	-
e	Adaptation ratio	0.957	0.237	0.014 ⁶	-	-

		Genotype	Age	Sex	Current	Current*Genotype
f	Average frequency, f	0.554	0.634	0.577	0.000	0.425
g	f_0	0.936	0.334	0.122	0.000	0.157
h	f_{ss}	0.666	0.650	0.578	0.000	0.977
i	AHP	0.774	0.659	0.434	0.000	0.656

965 Values are estimated p-values from the mixed linear model, n = 111 cells from 40 animals; for firing frequencies
 966 and AHP n = 67 cells from 26 animals. AP, action potential; ISI, interspike interval; adaptation ratio, first ISI/last
 967 ISI; f_0 , instantaneous firing frequency between two first APs; f_{ss} , instantaneous firing frequency between two
 968 last APs; AHP, afterhyperpolarization potential.

969 ¹Effect size: 2.5 mV ²Effect size: 1.7 mV (males lower) ³Effect size: 9.8 ms (males higher) ⁴Effect size: -0.07

970 ⁵Effect size: 0.07 (male higher) ⁶Effect size: 0.08 (male higher)

971

972 **Table 3.** Estimated marginal means and p-values for electrophysiological parameters of MEC II
 973 stellate cells. Basic electrophysiological properties of MEC LII stellate cells in homozygous transgenic
 974 rats (+/+) and negative control animals (-/-) for all cells are provided in Extended Data Table 3.1.
 975

		Estimated marginal means		p-values for test of fixed effects		
		-/-	+/+	Genotype	Age	Sex
a	Input resistance (MΩ)	50.3	55.5	0.327	0.762	0.133
b	Time constant, τ (ms)	13.3	13.3	0.945	0.121	0.004 ¹
c	Sag ratio	0.580	0.607	0.094	0.230	0.034 ²
d	Rebound (mV)	7.6	7.3	0.711	0.135	0.849
e	V_m (mV)	-64.7	-64.7	0.937	0.217	0.229
f	Resonance frequency (Hz)	4.5	4.5	0.982	0.025 ³	0.069
g	Rheobase (pA)	123	111	0.375	0.690	0.225
h	AP threshold (mV)	-47.9	-48.9	0.229	0.148	0.246
i	AP amplitude (mV)	89.1	86.4	0.105	0.231	0.974
j	AP half width (ms)	0.991	0.980	0.820	0.155	0.856
k	fAHP (mV)	-51.6	-53.1	0.034	0.000 ⁴	0.161
l	DAP (mV)	1.9	2.3	0.479	0.125	0.752

976 Values are estimated marginal means and p-values from the mixed linear model, n= 78 cells from 30 animals.

977 V_m , resting membrane potential; AP, action potential; fAHP, fast afterhyperpolarization potential; DAP,
 978 depolarizing afterpotential.

979 ¹Effect size: 2.2 ms (males lower) ²Effect size: 0.026 (males higher) ³Effect size: -0.65 Hz ⁴Effect size: -4.0 mV

980

981

982 **Table 4.** Estimated p-values for action potential parameters as a function of AP number and firing
 983 properties of MEC LII stellate cells.

		Genotype	Age	Sex	AP no	AP*Genotype
a	AP amplitude	0.318	0.463	0.812	0.000	0.258
b	AP width	0.264	0.670	0.246	0.000	0.589
c	ISI	0.576	0.593	0.977	0.000	0.685
d	ISI1/ISI2	0.449	0.657	0.416	-	-
e	Adaptation ratio	0.818	0.737	0.862	-	-
		Genotype	Age	Sex	Current	Current*Genotype
f	Average frequency, f	0.611	-	0.829	0.000	0.884
g	f_0	0.042	-	0.332	0.000	0.884
h	f_{ss}	0.839	-	0.870	0.000	0.984
i	AHP	0.561	-	0.629	0.000	0.922

984 Values are estimated p-values from the mixed linear model, n = 78 cells from 30 animals; for firing frequencies
 985 and AHP n = 38 cells from 16 animals. AP, action potential; ISI, interspike interval; adaptation ratio, first ISI/last
 986 ISI; f_0 , instantaneous firing frequency between two first APs; f_{ss} , instantaneous firing frequency between two
 987 last APs; AHP, afterhyperpolarization potential.

988

989

990

991 **Table 5.** Results from the mixed linear model for total number of activated pixels and PPR using VSDI
 992 in the DG of homozygous transgenic animals (+/+) and controls (-/-).

	Mean (SD)		p-values for test of fixed effects		
	-/-	+/+	Genotype	Sex	N (slices/animals)
Activated pixels					
(1 pulse)					
3 months	807 (284)	83 (297)	0.549	0.463	13/7
9 months	1698 (579)	1800 (279)	0.641	0.638	21/10
12 months	1687 (485)	1581 (427)	0.564	0.733	23/9
Paired-pulse ratio:					
Normal ACSF					
9 months	0.860 (0.098)	0.811 (0.032)	0.157	0.198	21/10
12 months	0.920 (0.119)	0.854 (0.098)	0.190	0.718	23/9
Paired-pulse ratio:					
Bicuculline					
9 months	1.320 (0.076)	1.321 (0.082)	0.970	0.897	15/8
12 months	1.373 (0.088)	1.363 (0.070)	0.859	0.782	15/9

993

994

995

996 **Table 6.** Results from the mixed linear model for quantified membrane potential change using VSDI
 997 in MEC of homozygous transgenic animals (+/+) and controls (-/-). Spread of activity from electrode
 998 placed in superficial layers MEC recorded with VSDI for all rats is shown in Extended Data Table 6.1.
 999

	p-values for test of fixed effects				
	Genotype	Sex	Distance from electrode	Distance from electrode * Genotype	N (slices/animals)
Superficial					
layers					
3 months	0.095	0.116	0.000	0.652	16/6
9 months	0.315	0.431	0.000	0.015	21/10
12 months	0.445	0.297	0.000	0.696	13/7
Across layers					
3 months	0.237	0.266	0.000	0.000	16/6
9 months	0.639	0.104	0.000	0.902	21/10
12 months	0.673	0.750	0.000	1.000	13/7

1000

1001

1002 **Extended Data**

1003

1004 **Table 1.1.** Basic electrophysiological and action potential properties of fan cells in LEC LII in

1005 homozygous transgenic rats (+/+) and negative control animals (-/-) at 1 and 3 months of age. A)

1006 Input resistance measured from a series of current steps. B) The membrane time constant, τ ; C) sag

1007 ratio; D) rebound potential; all measured from a current step of -300 pA. E) Resting membrane

1008 potential, V_m . F) Rheobase, measured by current steps increasing by 10 pA/step. G) Action potential

1009 threshold; H) action potential amplitude; I) action potential half width; all measured from the current

1010 step at rheobase. Values from all individual cells are shown (n = 111 cells in 40 animals).

1011

1012 **Table 2.1.** Action potential and firing properties of LEC LII fan cells in homozygous transgenic rats

1013 (+/+) and control animals (-/-), in both age groups. A) Action potential amplitude as a function of

1014 action potential number. B) Action potential width at 0mV as function of action potential number. C)

1015 ISI, interspike interval as a function of spike interval number. D) Ratio of the two first interspike

1016 intervals (ISI1/ISI2) and adaptation ratio (first ISI/ last ISI). Values in A-D are measured from a +200 or

1017 210 pA current (n = 111 cells in 40 animals). E) Average firing frequency, f ; F) instantaneous firing1018 frequency between two first spikes, f_0 ; G) instantaneous firing frequency between two last spikes, f_{ss} ;

1019 H) afterhyperpolarizing potential after end of current step; E-H are all plotted as a function of current

1020 (n = 67 cells in 26 animals). All values are shown as estimated marginal means and standard errors

1021 from the mixed linear model.

1022

1023

1024

1025 **Table 3.1.** Basic electrophysiological properties of MEC LII stellate cells in homozygous transgenic rats

1026 (+/+) and negative control animals (-/-) at 1 and 3 months of age. A) Input resistance measured from

1027 a series of current steps. B) The membrane time constant, τ ; C) sag ratio; D) rebound potential; all

1028 measured from a current step of -300 pA. E) Resting membrane potential, V_m . F) Membrane
 1029 resonance frequency in response to a ZAP current.

1030 G) Rheobase, measured by current steps increasing by 10 pA/step. H) Action potential threshold; I)
 1031 action potential amplitude; J) action potential half width; K) fAHP, fast afterhyperpolarization
 1032 potential; L) DAP, depolarizing afterpotential; all measured from the first action potential of the
 1033 current step at rheobase. Values from all individual cells are shown (n = 78 cells in 30 animals).

1034

1035 **Table 4.1.** Action potential and firing properties of MEC LII stellate cells in homozygous transgenic
 1036 rats (+/+) and control animals (-/-), for both age groups in A-D, 1 month group in E-H. A) Action
 1037 potential amplitude as a function of action potential number. B) Action potential width at 0 mV as
 1038 function of action potential number. C) ISI, interspike interval as a function of spike interval number.
 1039 D) Ratio of the two first interspike intervals (ISI1/ISI2) and adaptation ratio (first ISI/ last ISI). Values
 1040 in A-D are measured from a +200 pA current step (n = 78 cells in 30 animals). E) Average firing
 1041 frequency, f ; F) instantaneous firing frequency between two first spikes, f_0 ; G) instantaneous firing
 1042 frequency between two last spikes, f_{ss} ; H) Afterhyperpolarizing potential after end of current step; E-
 1043 H are all plotted as a function of current (n = 38 cells in 16 animals). All values are shown as
 1044 estimated marginal means and standard errors from the mixed linear model.

1045

1046

1047

1048 **Figure 5.1.** Results from the mixed linear model for quantified membrane potential change using
 1049 VSDI in the DG of homozygous transgenic animals (+/+) and controls (-/-).

p-values for test of fixed effects				
Genotype	Area	Genotype x Area	Sex	N (slices/animals)
1 pulse				

a	3 months	0.177	0.008	0.316	0.753	13/7
b	9 months	0.757	0.014	0.583	0.022	21/10
c	12 months	0.191	0.243	0.019	0.192	23/9
4 pulses						
d	9 months	0.28	0.017	0.68	0.005	21/10
e	12 months	0.394	0.208	0.007	0.169	23/9
Bicuculline						
f	9 months	0.155	0.069	0.197	0.496	15/8
g	12 months	0.596	0.066	0.016	0.596	15/9

1050

1051 **Table 6.1.** Spread of activity from electrode placed in superficial layers MEC recorded with VSDI in

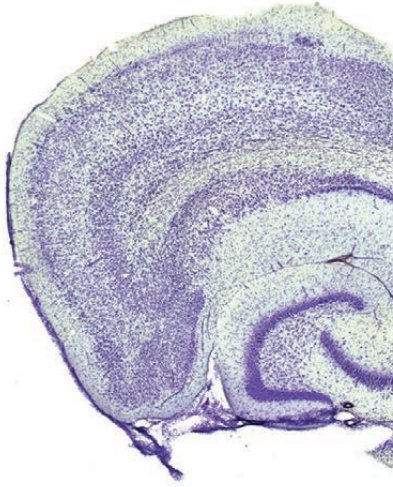
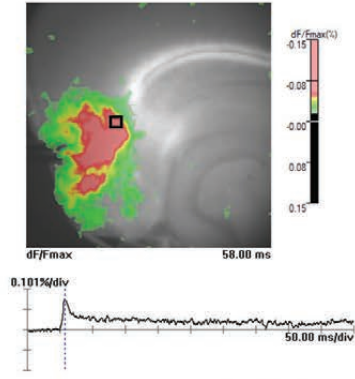
1052 wild type (wt) and transgenic (+/+) rats. The relative membrane potential change at increasing

1053 distance from the electrode tip is shown within the superficial layers (left) and across the layers of

1054 MEC (right), for 3, 9 and 12 months old rats.

1055

A



B

